metals

Article

Superconductivity in ZrB_{12} under High Pressure

Zexiao Zhang [1], Xu Zheng [1,*], Hanshan Luo [1], Chan Gao [1], Xiaowei Xue [1], Jingcheng Zhu [1], Ruobin Li [1], Changqing Jin [2] and Xiaohui Yu [2]

[1] Department of Physics, Chengdu University of Technology, Chengdu 610059, China; 2023021166@stu.cdut.edu.cn (Z.Z.); 19822962579@163.com (H.L.); gaochan@ustc.edu.cn (C.G.); xxw2243346192@gmail.com (X.X.); a1659022429@outlook.com (J.Z.); l17798346938@hotmail.com (R.L.)

[2] Beijing National Laboratory for Condensed Matter Physics, Institute of Physics, Chinese Academy of Sciences, Beijing 100190, China; jin@iphy.ac.cn (C.J.); yuxh@iphy.ac.cn (X.Y.)

* Correspondence: zhengxu@cdut.edu.cn

Abstract: Transition metal borides have emerged as pivotal players in various fields. In addition to their exceptional properties such as high hardness, a high melting point, and corrosion resistance, certain compounds exhibit remarkable characteristics including superconductivity, magnetism, electrical conductivity, and catalytic activity. Among these compounds, ZrB_{12} has garnered significant attention due to its unique physicochemical properties. However, previous research on ZrB_{12} has predominantly focused on its mechanical behavior while overlooking the electron-electron interactions of the superconducting state. In this paper, resistance characterization of ZrB_{12} under high-pressure conditions was conducted to further investigate its superconductivity. Our research findings indicate that ZrB_{12} maintains its superconductivity within a pressure range of 0 to 1.5 GPa and is classified as a type 2 superconductor. Additionally, the results confirm the anisotropic nature of ZrB_{12}'s superconductivity. As the pressure increases, the superconducting transition temperature undergoes a gradual decrease. Remarkably, ZrB_{12} exhibits metallic behavior under pressures up to 31.4 GPa. The observed decline in superconductivity in ZrB_{12} can be ascribed to the intensified influence of Zr's movement on phonon dispersion, ultimately leading to a reduction in carrier concentration.

Keywords: transition metal borides; hard material; superconductivity; high pressure; zirconium dodecaboride

check for updates

Citation: Zhang, Z.; Zheng, X.; Luo, H.; Gao, C.; Xue, X.; Zhu, J.; Li, R.; Jin, C.; Yu, X. Superconductivity in ZrB_{12} under High Pressure. *Metals* **2024**, *14*, 1082. https://doi.org/10.3390/met14091082

Academic Editor: Jiro Kitagawa

Received: 15 August 2024
Revised: 14 September 2024
Accepted: 19 September 2024
Published: 21 September 2024

1. Introduction

The rapid progress of industrialization worldwide has led to the extensive utilization of hard materials in various fields, including weaponry, aviation, machinery, construction, geological exploration, and mining [1,2]. Traditionally, hard materials are composed of compounds featuring shorter covalent bonds centered around lighter elements with smaller atomic radii, such as boron, carbon, nitrogen, and oxygen. However, due to the limitations of traditional hard materials in terms of mechanical and electrical properties, there is a growing interest in exploring novel hard materials comprising compounds formed from light elements and transition metals [3,4]. Due to the high density and large bulk modulus of transition metals, the doping of light elements can be carried out with the *d*-orbital of transition metals to form quasi-covalent bonds [5], significantly enhancing the hardness. Moreover, the distribution of the *d*-orbitals of transition metals in the outer space of the nucleus is more complex compared to the traditional superhard materials. Therefore, these materials frequently form diverse structures, exhibiting exceptional properties and potential benefits for substituting conventional hard materials in domains such as electronics, information technology, and aerospace [6].

Significant advancements have been achieved in recent years regarding the investigation of transition metal borides. In addition to high hardness, a high melting point, and strong corrosion resistance similar to traditional superhard materials, certain compounds also exhibit properties such as superconductivity [7], magnetism, electrical conductivity [8], and catalysis [9]. Transition metal borides have emerged as extensively investigated among the transition metals, owing to their finely dispersed powder form and their proclivity to readily react with metals under relatively moderate conditions. This reactivity leads to the formation of a diverse range of stable compounds. ZrB_{12}, as a noteworthy representative of this category, has garnered significant attention due to its remarkable physicochemical properties. The experiments and first-principles calculations on ZrB_{12} show that the symmetrical B-B covalent network can form delocalized π-bonds, and the interaction of the *4d*-orbitals of Zr atoms with these π-bonds creates electronic channels, thereby maintaining the material's ultrahardness while also providing good electrical conductivity [10–12]. Notably, heavily doped ZrB_{12} has a calculated hardness of up to 40 GPa [13,14], while its superconducting transition temperature approaches 6 K [15]. Singularly, ZrB_{12} exhibits a range of behaviors that deviate significantly from the typical characteristics observed in conventional superconductors. Several theoretical models have been proposed to elucidate its superconducting properties, each offering a distinct perspective on the nature of this intriguing material. One such model characterizes ZrB_{12} as a traditional superconductor with amplified surface effects that could be responsible for its unique behavior [16,17]. Another model suggests that ZrB_{12} possesses a strongly coupled *s*-wave gap structure [18], while another intriguing proposal posits that it may exhibit *d*-wave superconductivity. The temperature-dependent behavior of the magnetic penetration depth in ZrB_{12} reveals a pronounced two-band structure feature [19], which implies that the interaction between these bands is relatively weak [20]. Recent band structure calculations have determined that the Fermi surface of ZrB_{12} consists of both an open sheet and a closed sheet [21], which is a characteristic that could underpin the observed multiband nature of its superconductivity. Additionally, specific heat and vortices measurements consistent with both type 1 and type 2 superconducting behaviors [22,23]. Zhang et al. provided further insight by confirming, through the use of X-ray diffraction techniques, that ZrB_{12} belongs to the category of type 1.5 superconductivity [24,25]. These results suggest that ZrB_{12} may represent a distinct class of superconductors, inherently capable of simultaneously exhibiting both type 1 and type 2 characteristics simultaneously. Therefore, the contribution of electron–electron interactions in ZrB_{12} is expected to be substantial. However, recent research on ZrB_{12} has predominantly focused on the superconducting type, with limited attention given to investigating the electron–electron interactions in the superconducting character. This intriguing possibility has piqued our interest and motivated us to further explore the superconducting properties of ZrB_{12}, particularly through the application of high-pressure techniques.

Applying pressure can often effectively change the electronic structure of compounds, and even induce phase transitions, without introducing additional impurities [26,27]. In this study, we conducted resistance characterization under pressure to investigate electron–electron interactions in the superconductor ZrB_{12}. Encouragingly, ZrB_{12} exhibits exceptional stability with minimal structural impact even at pressures as high as 44 GPa, thereby preserving its phase integrity [28,29]. Our research reveals that the superconductivity of ZrB_{12} exhibits anisotropic characteristics, which persist even under high-pressure conditions. Furthermore, under a pressure of 1.5 GPa, ZrB_{12} still exhibits superconductivity at approximately 5.7 K. With increasing pressure, the superconducting transition temperature decreases. ZrB_{12} exhibits metallic behavior under pressures up to 31.4 GPa. The diminishing superconductivity observed in ZrB_{12} can be attributed to the intensified effect of Zr's movement on phonon dispersion, ultimately causing a reduction in carrier concentration.

2. Materials and Methods

High-purity Zr (>99.95%) and B (>99.99%) powders in the molar ratio of Zr:B = 1:12 were homogeneously mixed and compacted into cylindrical pellets. Subsequently, the cylinder was placed within a BN thermal insulation layer, which was further enclosed in a graphite furnace. As pyrophyllite has low hardness, good slippage, insulation, sealing, high temperature resistance, and good heat preservation performance, it is suitable as a pressure transmission medium. The assembly was put into a cubic press where the reactants were gradually heated to 2000 °C (5 °C/min) under a pressure of 5.5 GPa for 15 min to obtain stable ZrB_{12}.

The products were washed with distilled ethyl alcohol to remove the impurities, followed by drying in an oven at 348 K. We used a 6 × 600 t high-pressure machine and pyrophyllite as the pressure medium. The method of pressure measurement is conducted based on the variation in metal resistance during solid-to-solid phase transition under different pressures. In this paper, we used Bi (I–II) and Ba (II–III) phase transitions. The pressure of the sample corresponding to the pressure points of 2.55 GPa and 5.5 GPa can be obtained through the metals Bi and Ba. The internal diagram of the 6 × 600 t high-pressure machine is shown in Figure S1. The typical process is as follows: firstly, the pressure is elevated to the desired value; once the pressure is stable, the heating procedure is started until the required temperature is reached. Depending on specific synthesis conditions, diverse sample assembly configurations can be employed within six WC anvils.

The symmetries of different crystal orientations for a given type of crystal can be utilized to determine their respective orientations. In the case of ZrB_{12} single crystals, their orientation is primarily determined using the Laue method. The method requires the data acquisition plate to be in front of the sample and perpendicular to the incident X-ray, with the sample positioned 40 mm higher than the plate. Figure S2 shows the Laue diffraction of [110] (dyad symmetry) and [100] (quadruple symmetric). The single-crystal cutting method involves using a low-speed cutting machine to precisely cut along the single-crystal orientation. By aligning the crystal orientation parallel to the saw blade of the cutting machine, crystals with various orientations can be obtained.

The electronic transport properties of a [100]-oriented ZrB_{12} single crystal with high pressure up to 44 GPa were measured using four-probe electrical conductivity methods in a CuBe alloy diamond anvil cell (DAC). The diamond culet had a diameter of 300 μm, and Au wires with a diameter of 18 μm were used as electrodes. A T_{301} stainless steel gasket was compressed to a thickness of 20 μm with a 150 μm diameter hole, into which the cubic BN was pressed as an insulating layer. A small center hole of 100 μm in diameter was drilled to serve as the sample chamber, where NaCl fine powder served as a pressure-transmitting medium. A piece of ZrB_{12} single crystal measuring 50 μm × 50 μm × 25 μm was loaded into this chamber along with a ruby for pressure measurement. Heat capacity measurements on single crystalline samples 1 × 1 × 0.5 mm^3 in size were carried out on a PPMS (QD China, Beijing, China).

High-P synchrotron X-ray diffraction experiments using a DAC were performed at the Beijing Synchrotron Radiation Facility (BSRF), Beijing, China. The obtained polycrystalline ZrB_{12} was ground into powders and loaded into the sample hole in a stainless steel gasket with neon as the pressure-transmitting medium. A few ruby balls were also loaded into the same sample chamber to serve as an internal pressure standard. The collected angle-dispersive diffraction data were analyzed by integrating 2D images as a function of 2θ using the program Fit2D to obtain the conventional, one-dimensional diffraction profiles.

3. Results

ZrB_{12} crystallizes in a cubic crystal system characterized by the space group *Fm-3m*, which is assigned the number 225 in the International Tables for Crystallography. Within this symmetrical framework, the Zr atoms are located at specific Wyckoff positions, which are designated sites within the unit cell that can be occupied by atoms or ions. The Zr atoms are surrounded by clusters of boron atoms, forming B_{12} icosahedra. These B_{12} clusters form a rigid, three-dimensional network that contributes to the exceptional properties of ZrB_{12}, including a high melting point and excellent thermal conductivity. The cubic arrangement with B_{12} clusters renders ZrB_{12} a material of significant interest for various high-temperature and high-strength applications [30]. The Zr atoms in ZrB_{12} have an electron configuration of $4s^2 4p^6 4d^3 5s^1$ and the B atoms have $2s^2 2p^1$, which serve as valence electrons. These contribute to covalent bonding, thereby fulfilling the characteristics of ultra-hard materials, including a high average valence electron count per atom, a maximal number of covalent bonds per unit volume, and a high bond energy. In order to investigate the electrical transport properties under external pressure on ZrB_{12}, we measured temperature dependence resistance from 2 to 300 K for both [110] and [100] orientations of a ZrB_{12} single crystal, as shown in Figure 1a. Here, the T_c^{onset} is determined as the interception between two straight lines below and above the superconducting transition, while T_c^{zero} is defined as the zero-resistivity temperature. As the temperature decreases, the T_c^{onset} for the [100] and [110] is 5.8 K and 5.7 K, whereas the T_c^{zero} is 4.6 K and 3.4 K, respectively [31]. Moreover, the resistivity has a certain difference, and the resistivity in the [100] orientation is significantly greater than that of the [110] orientation. These findings demonstrate the anisotropic electrical behavior of ZrB_{12}, which is consistent with prior research reports [13]. The specific heat measurements of the [100] orientation below 10 K reveal a peak heat capacity within the weak magnetic field near 0 T, as shown in Figure 1b. An exothermic process around 5.4 K was confirmed, providing further evidence for a superconducting transition around this temperature [15,32]. In ZrB_{12}, which is classified as a two-gap superconductor exhibiting dynamic charge stripes, the interplay between these fluctuating charges and magnetic vortices can occur even under relatively low magnetic fields. This interaction induces a pronounced anisotropy in the superconducting properties of the material. Specifically, the behavior of the superconducting characteristics, such as the critical temperature and the critical current density, becomes highly dependent on the orientation of the applied magnetic field. This anisotropy is a direct consequence of the dynamic charge stripe order within the superconductor, which modulates the electronic structure and thereby influences the pinning and motion of vortices within the material. Bolotina et al. show a stepped singularity of the specific heat capacity of the [100] and [110] crystal orientations at around 5.8 K, and another hump of the [110] orientation appeared at around 5.7 K, demonstrating the band-gap anisotropy of ZrB_{12} single crystals [33]. Generally, the resistivity of ZrB_{12} will immediately approach 0 upon reaching the first superconducting temperature. Therefore, in our resistivity experiment, we can only observe the tendency of the resistivity drop to zero and cannot observe the second peak of the [110] orientation. The presence of such a pronounced anisotropy in the superconducting behavior of ZrB_{12} highlights the intricate relationship between the charge stripe fluctuations and the vortex dynamics, and it underscores the complexity of the superconducting state in materials with this unique electronic structure [33]. Consequently, the change in the heat capacity under the magnetic field, the magnitude of the resistivity, and the differences in the superconducting temperature collectively confirm the anisotropy of ZrB_{12}.

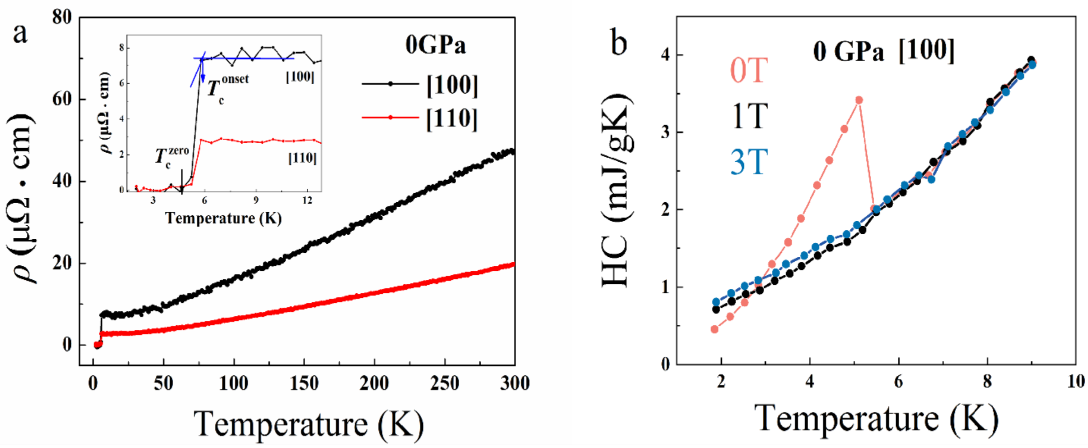

Figure 1. (**a**) Temperature dependence of [100] and [110] orientation resistivity at 2 to 300 K under 0 GPa. Inset figure is superconducting temperature of ZrB_{12} single crystal. (**b**) Specific heat capacity of ZrB_{12} from 2 to 9 K under magnetic fields of 0 T, 1 T, and 3 T.

Furthermore, we characterized the temperature dependence of resistance for a ZrB_{12} single crystal with the [100] orientation at 1.5 GPa under an external magnetic field ranging from 0 to 1 T (as shown in Figure 2). As shown in Figure 2a, the T_c^{onset} at 0.05, 0.1, 0.15, 0.2, 0.25, and 0.3 T is 5.4, 5.0, 4.7, 4.3, 3.9, and 3.5 K, while the corresponding T_c^{zero} values are 3.2, 2.8, 2.1 K, respectively. T_C decreases with an increasing applied magnetic field H, and this variation is illustrated in Figure 2b. Using the Werthamer–Helfand–Hohenberg (WHH) formula,

$$H_{c2}(0) = -0.693T_{c0} \times \left(\frac{dH_{c2}}{dT} |T_{c0} \right) \tag{1}$$

where T_{c0} is the superconducting transition temperature under zero magnetic field. At 1.5 GPa, the upper critical field $H_{c2}(0)$ was estimated to be 0.64 T. From Figures 1b and 2a, it is apparent that the intensification of the magnetic field to 1 Tesla completely suppresses superconductivity, indicating that the [100] orientation of the ZrB_{12} single crystal belongs to the classification of type 2 superconductivity. Based on the Ginzburg–Landau theory, Abrikosov categorized superconductors into two distinct types: type 1 and type 2, according to the magnitude of the Ginzburg–Landau parameter. ZrB_{12} has been proposed to exhibit a two band-effect and related type 1.5 superconductivity (containing type 1 and type 2) by using X-ray diffraction and μSR studies [26,34]. The observation of type 2 superconductivity presented in Figure 2b does not contradict the conclusion of type 1.5 superconductivity, as the type 1.5 superconductivity of ZrB_{12} can only be observed below T_c, whereas our discussion primarily focuses on the relationship between T_c and the magnetic field H. We take into account the anisotropy along the [100] direction, which restricts our observations solely to type 2 superconductivity. Furthermore, as illustrated in Figure 2a, at relatively low magnetic fields and below T_c, the superconducting transition exhibits a remarkably sharp profile. As the magnetic field intensifies, the transition gradually broadens, which may be attributed to various vortex phase transitions [26]. Figure 2b shows the characteristic of the upper critical field $H_{c2}(0)$ in type 2 superconductors, which provides insight into the microscopic mechanism of ZrB_{12}. Generally, two independent mechanisms govern the suppression of superconductivity by magnetic fields. One involves the orbital pair breaking of Cooper pairs in the superconducting state, which is associated with screening currents that exclude the external field which is commonly referred to as the orbital limit. The other mechanism is a spin effect resulting from Zeeman splitting, which is applicable only to singlet pairings and is widely known as the Pauli paramagnetic limit. Evidently, ZrB_{12} aligns with the former theoretical explanation.

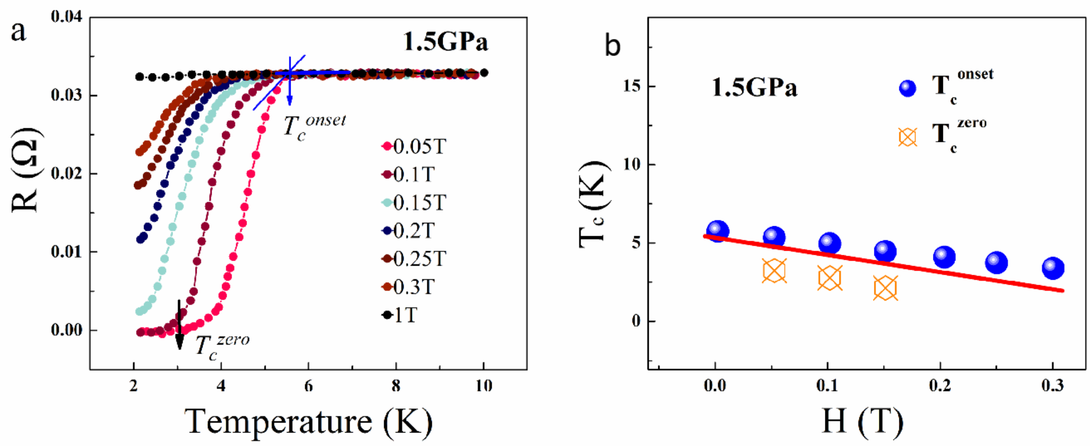

Figure 2. (**a**) The [100] orientation superconducting transition temperature dependence of the magnetic field at 0 T, 0.05 T, 0.1 T, 0.15 T, 0.2 T, 0.25 T, 0.3 T under 1.5 GPa. (**b**) The relationship between the [100] orientation superconducting transition temperature and the magnetic field under 1.5 GPa.

In order to comprehensively investigate the electrical transport properties within a high-pressure environment, it is imperative to ensure and validate the structural stability of the ZrB_{12} compound under compressive forces, without experiencing any detrimental alterations or deformations. This validation is crucial because the stability of ZrB_{12}'s crystal lattice directly impacts its ability to effectively conduct electricity under such extreme conditions, thereby influencing the reliability and accuracy of measurements pertaining to electrical transport properties. A high-pressure synchrotron X-ray diffraction (λ = 0.6199 Å) study conducted in a DAC was used to investigate the phase stability of ZrB_{12}. Figure 3a presents the XRD patterns obtained during ambient-temperature compression, revealing that the ZrB_{12} single crystal sustains its structural stability up to 43 GPa, without any observable phase transition. The lattice parameters of ZrB_{12} in Figure 3b exhibit a nearly linear decrease with increasing pressure. In Figure S3, the pressure–volume data for ZrB_{12} demonstrate a gradual reduction in both the lattice parameters and volume as pressure increases. This can be attributed to the compression of atomic distances under elevated pressures, resulting in enhanced repulsive interactions among atoms and consequently higher crystal incompressibility. The Zr atomic radius is significantly larger than that of B, the interplanar spacing of ZrB_{12} gradually decreases under pressure, and the influence on the orbital of Zr is much greater than that of B. Therefore, on the premise of ensuring the structural stability of ZrB_{12} under pressure, our research on the high-pressure behavior of ZrB_{12} primarily focuses on investigating alterations in the Zr-*d* atomic orbital. The third-order Birch–Murnaghan equation of state (EOS) was employed to fit the ZrB_{12} unit cell, resulting in a bulk modulus B = 221.1 GPa, as illustrated in Figure S3, which demonstrates its compressibility. Therefore, it can be concluded that ZrB_{12} maintains its structural stability under high pressure. Subsequently, we investigated the electrical transport characteristics of ZrB_{12} single crystals under pressures ranging from 4.4 to 44 GPa, as depicted in Figure 4. Specifically, Figure 4a exhibits the [100] orientation resistance–temperature curves from 2 to 300 K across 4.4 to 20 GPa, with an inset figure presenting these curves normalized between 2 and 10 K. The obtained data clearly demonstrate that as pressure increases, ZrB_{12} consistently maintains its superconducting state, while exhibiting a decrease in T_c. Furthermore, under pressures ranging from 31.4 to 44 GPa, ZrB_{12} exhibits metallic behavior, as illustrated in Figure 4b.

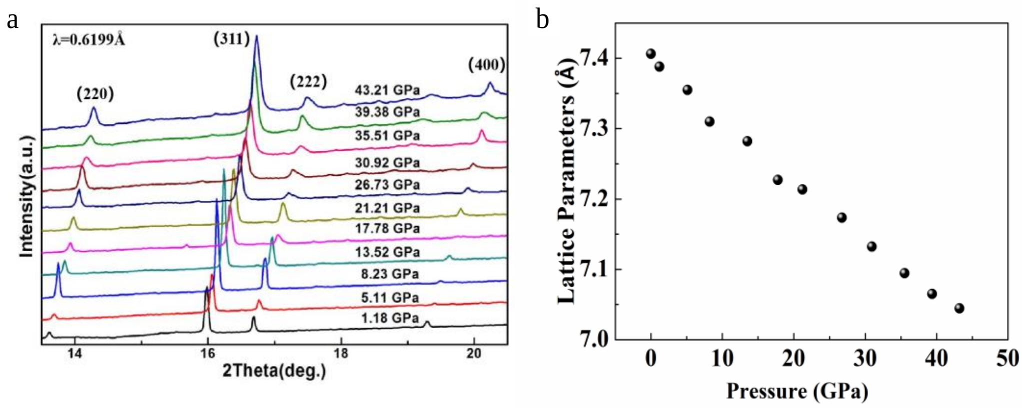

Figure 3. (**a**) High-pressure XRD patterns collected at room temperature. (**b**) Lattice parameters of ZrB_{12} under high pressure.

Figure 5 presents the phase diagram of the superconducting transition temperature (SC) dependence pressure of ZrB_{12}, illustrating a region of gradual decrease in T_c^{onset} and T_c^{zero} from 0 to 44 GPa. The relationship between the superconducting transition temperature and pressure exhibits a gradual decline with a slope of approximately 0.236 K/GPa. From the phase diagram, we can easily visualize the evolution and intimated correlations between the metal and SC as a function of pressure. As pressure increases gradually, T_c^{onset} is suppressed, accompanied by an initial enhancement of T_c with a broad superconducting transition width, as displayed in Figure 4a. Interestingly, our observations under applied pressure indicate that despite the absence of structural phase transition in ZrB_{12} under elevated pressures, the superconducting transition temperature disappears at 20 GPa, coinciding with an increase in pressure. This phenomenon exhibits a metallic behavior, which is strongly associated with the electron–electron interaction within the single crystal.

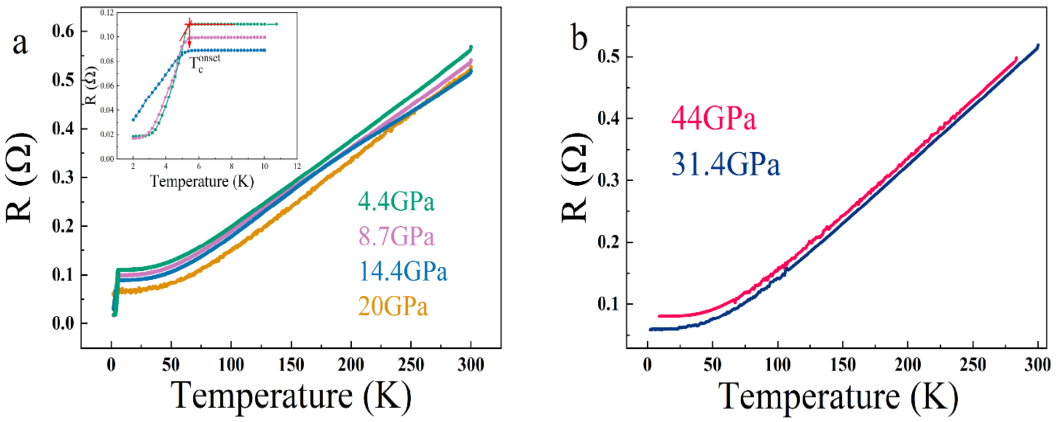

Figure 4. (**a**) The [100] orientation resistance–temperature curves from 2 to 300 K under 4.4 to 20 GPa. (**b**) The [100] orientation resistance–temperature curve at pressures ranging from 31.4 to 44 GPa.

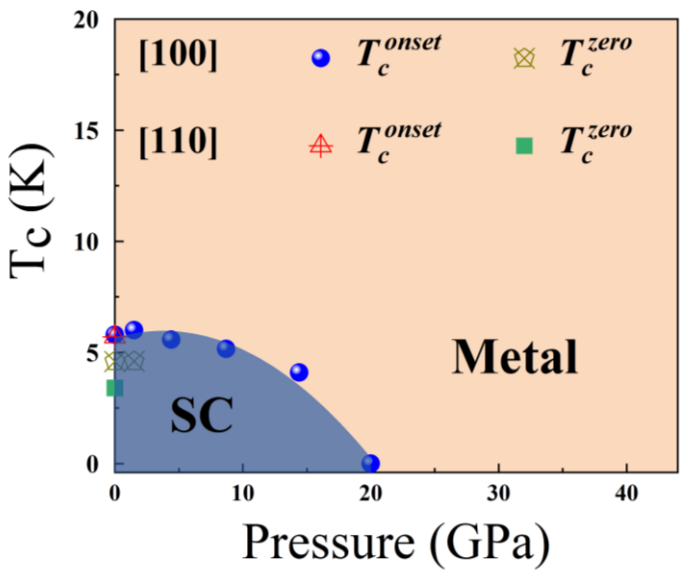

Figure 5. The phase diagram of superconducting transition temperature (SC) dependence pressure of ZrB_{12}.

4. Discussion

The exceptional hardness exhibited by ZrB_{12} can be largely attributed to the presence of strong covalent bonds between the boron atoms within its crystalline structure. These B-B covalent bonds are a direct consequence of the unique integration and interaction of boron elements within the framework of transition metals, specifically Zr. The robustness of these bonds significantly contributes to the overall hardness of the ZrB_{12} crystal, rendering it a material of interest in various high-performance applications where resistance to wear and deformation is crucial. The existence and positioning of Zr atoms play a crucial and indispensable role in facilitating and enhancing the electrical conductivity and superconducting capabilities of this specific material. Furthermore, under conditions of zero pressure, it is observed that there is a complete absence of energetic interaction or overlap between the optical phonon modes and the acoustic phonon modes [35]. This intriguing phenomenon can be attributed to the distinct and varying atomic masses of Zr atoms and B atoms as they are arranged within the crystal lattice unit cell. The disparity in their masses ensures that the vibrational modes associated with these atoms do not intersect energetically, thereby maintaining a clear separation between the two types of phonon modes. This separation is essential for the material to exhibit its unique electrical properties, particularly its ability to conduct electricity and transition into a superconducting state under specific conditions [35]. As pressure rises, ZrB_{12} exhibits remarkable resistance to compression, which is attributed to the robust B-B covalent bond. The band structure of ZrB_{12} remains largely unaltered, with the primary variations originating from the Zr atomic orbital. Consequently, our focus lies in exploring the disappearance of superconductivity resulting from the electronic–electron interactions in ZrB_{12} under pressure, along with the corresponding changes in the Zr atomic orbital. The electronic density of states (DOS) and the partial density of states (PDOS) of ZrB_{12} at 0 GP demonstrated that the DOS at the Fermi level is predominantly dominated by Zr-*d* states. This indicates that the electron carriers in ZrB_{12} originate primarily from the Zr-*d* states. In addition, the changes in cell parameters and volume with pressure derived from our experimental values (as shown in Figures 3 and S3) are basically consistent with the theoretical calculated values of Li, X. et al. [35]. According to the calculation results of ZrB_{12} by Li, X. et al., the DOS of ZrB_{12} at 0, 20, 50 GPa was 1.4679 eV, 1.4001 eV, and 1.3571 eV, respectively. When the pressure is below 50 GPa, the carrier concentration gradually decreases under the action of pressure and reaches the minimum value at 50 GPa, indicating that ZrB_{12} exhibits limited compressibility due to its high bulk modulus. In general, in the case of internal stability of ZrB_{12} the change in carrier concentration and resistance are correlated. As can be seen from Figure 4a, the resistance of our sample gradually decreases under the applied pressure. However, from Figure 4b, when the pressure is further increased to 44 GPa, ZrB_{12} exhibits significant resistance to compression, with a resistance level similar to that observed at 31.4 GPa, indicating that the change in carrier concentration during this stage is relatively small and gradually reaches a minimum value. These results are consistent with the calculated value. As the pressure increases, the contribution of Zr movement to phonon dispersion becomes more significant [35]. With the growing influence of Zr's movement on phonon dispersion, it may result in a reduction in carrier concentration. Therefore, within the pressure range of 0 to 44 GPa, the carrier concentration of ZrB_{12} steadily decreases as pressure rises. This reduction in carrier concentration leads to a decrease in its superconducting transition temperature. Lower carrier concentrations require even lower temperatures for achieving superconducting transition. Notably, at 20 GPa, the superconducting transition was undetectable, suggesting orbital pair breaking of Cooper pairs in the superconducting state of ZrB_{12}, thereby indicating a transition to a metallic state.

5. Conclusions

In summary, previous research has primarily focused on the mechanical and structural properties of ZrB_{12}, with limited attention given to electron–electron interactions in the superconducting character. In this paper, we discuss the electrical transport properties of ZrB_{12} single crystals under high-pressure conditions. Our findings reveal that ZrB_{12} single crystal superconductivity is anisotropic, which persists even under high pressure. Under a pressure ranging from 0 to 1.5 GPa, ZrB_{12} (crystal orientation of [100]) maintains its superconducting nature and is classified as a type 2 superconductor. At 1.5 GPa, the upper critical field $H_{c2}(0)$ was estimated to be 0.64 T. With increasing pressure, the superconducting transition temperature decreases. At 20 GPa, no evidence of superconducting transition was observed. The metallic behavior of ZrB_{12} remains evident under pressures ranging from 31.4 to 44 GPa. To further delve into the superconducting properties of ZrB_{12}, we conducted an in-depth analysis of its crystal structure and electronic interactions by a phase diagram of the superconducting transition temperature dependence pressure of ZrB_{12}. Within the ZrB_{12} crystal lattice, the crucial presence of Zr atoms enables the conduction and superconductivity properties of this material, with electron carriers primarily originating from the Zr-*d* states. As the pressure escalates, the contribution of Zr movement to phonon dispersion becomes increasingly significant. This enhanced influence of Zr's movement on phonon dispersion may result in a decrease in carrier concentration. Consequently, within the pressure range of 0 to 44 GPa, the carrier concentration of ZrB_{12} progressively diminishes as the pressure rises. This decrement in carrier concentration leads to a corresponding decline in its superconducting transition temperature, requiring even lower temperatures for the occurrence of superconducting transition. Notably, at 20 GPa, the superconducting transition becomes undetectable, indicating orbital pair breaking of Cooper pairs in the superconducting state of ZrB_{12}, thus signifying a transition to a metallic state.

To gain a deeper understanding of the superconducting mechanisms in ZrB_{12}, further studies are needed to investigate the electronic structure, phonon dispersions, and electron–phonon coupling under pressure. Such studies would provide valuable insights into the nature of superconductivity in ZrB_{12} and potentially lead to the discovery of new superconductors with enhanced properties.

Supplementary Materials: The following supporting information can be downloaded at: https://www.mdpi.com/article/10.3390/met14091082/s1, Figure S1: The internal diagram of the 6 × 600 t high- pressure machine.; Figure S2: Laue diffraction of (a) [110] and (b) [100] orientation; Figure S3: The pressure—volume data for ZrB_{12} and equation of state analysis.

Author Contributions: Conceptualization, X.Z. and X.Y.; Methodology, Z.Z.; Validation, Z.Z., H.L., X.X., J.Z. and R.L.; Investigation, Z.Z., H.L., X.X., J.Z. and R.L.; Resources, X.Z., C.G., C.J. and X.Y.; Data curation, Z.Z.; Writing—original draft preparation, Z.Z.; Writing—review & editing, X.Z., C.G., C.J. and X.Y.; Visualization, X.Z., C.G., C.J. and X.Y. All authors have read and agreed to the published version of the manuscript.

Funding: This study were partially supported by Sichuan Science and Technology Program (No. 2023NSFSC1371)and Chengdu University of Technology 2023 Young and Middle-aged Backbone Teachers Development Funding Program (No. 10912-JXGG2023-09014).

Data Availability Statement: The original contributions presented in the study are included in the article/supplementary material, further inquiries can be directed to the corresponding author/s.

Acknowledgments: The authors would like to express their gratitude to the Synergic Extreme Condition User Facility (SECUF) for its invaluable support in several laboratory experiments.

Conflicts of Interest: The authors declare no conflicts of interest.

References

1. Haines, J.; Léger, J.M.; Bocquillon, G. Synthesis and design of superhard materials. *Annu. Rev. Mater. Res.* **2001**, *31*, 1–23. [CrossRef]
2. Xu, B.; Tian, Y. Ultrahardness: Measurement and enhancement. *J. Phys. Chem. C* **2015**, *119*, 5633–5638. [CrossRef]
3. Qiao, Z.; Ma, X.; Zhao, W.; Tang, H. High-pressure sintering the novel light ($W_{0.25}Al_{0.75}$)C hard material without binder phase. *J. Alloys Compd.* **2009**, *472*, 211–213. [CrossRef]
4. Zhang, S.F.; Zhou, C.; Sun, G.Q.; Wang, X.; Bao, K.; Zhu, P.W.; Zhu, J.M.; Wang, Z.Q.; Zhao, X.B.; Tao, Q.; et al. Electronic structure and hardness of Mn_3N_2 synthesized under high temperature and high pressure. *Metals* **2022**, *12*, 2164. [CrossRef]
5. Prosviryakov, A.; Mondoloni, B.; Churyumov, A.; Pozdniakov, A. Microstructure and hot deformation behaviour of a novel Zr-alloyed high-boron steel. *Metals* **2019**, *9*, 218. [CrossRef]
6. Xu, B.; Tian, Y. Superhard materials: Recent research progress and prospects. *Sci. China Mater.* **2015**, *58*, 132–142. [CrossRef]
7. Nagamatsu, J.; Nakagawa, N.; Muranaka, A.; Znan, Y.; Akmsu, J. Superconductivity at 39 K in magnesium diboride. *Nature* **2001**, *410*, 63–64. [CrossRef]
8. Kayhan, M.; Hildebrandt, E.; Frotscher, M.; Senyshyn, A.; Albert, B. Neutron diffraction and observation of superconductivity for tungsten borides, WB and W_2B_4. *Solid State Sci.* **2012**, *14*, 1656–1659. [CrossRef]
9. Zhu, J.; Cannizzaro, F.; Liu, L.; Zhang, H.; Kosinov, N.; Filot, I.; Rabeah, J.; Brückner, A.; Hensen, E. Ni–In synergy in CO_2 hydrogenation to methanol. *ACS Catal.* **2021**, *11*, 11371–11384. [CrossRef]
10. Gasparov, V.A.; Sidorov, N.S.; Zver'kova, I.I.; Khassanov, S.S.; Kulakov, M.P. Electron transport, penetration depth, and the upper critical magnetic field in ZrB_{12} and MgB_2. *J. Exp. Theor. Phys.* **2005**, *101*, 98–106. [CrossRef]
11. Paderno, Y.B.; Adamovskii, A.A.; Lyashchenko, A.B.; Paderno, V.N.; Fillipov, V.B.; Naydich, Y.V. Zirconium dodecaboride-based cutting material. *Powder Metall. Met. C* **2004**, *43*, 546–548. [CrossRef]

12. Post, B.; Glaser, F.W. Crystal structure of ZrB_{12}. *JOM* **1952**, *4*, 631–632. [CrossRef]
13. Ma, T.; Li, H.; Zheng, X.; Wang, S.; Wang, X.; Zhao, H.; Han, S.; Liu, J.; Zhang, R.; Zhu, P.; et al. Ultrastrong boron frameworks in ZrB_{12}: A highway for electron conducting. *Adv. Mater.* **2017**, *29*, 1604003. [CrossRef]
14. Pan, Y.; Chen, S. Influence of alloying elements on the mechanical and thermodynamic properties of ZrB_2 boride. *Vacuum* **2022**, *198*, 110898. [CrossRef]
15. Papaconstantopoulos, D.A.; Mehl, M.J. First-principles study of superconductivity in high-pressure boron. *Phys. Rev. B* **2002**, *65*, 172510. [CrossRef]
16. Tsindlekht, M.I.; Leviev, G.I.; Asulin, I.; Sharoni, A.; Millo, O.; Felner, I.; Paderno, Y.B.; Filippov, V.B.; Belogolovskii, M.A. Tunneling and magnetic characteristics of superconducting ZrB_{12} single crystals. *Phys. Rev. B* **2004**, *69*, 212508. [CrossRef]
17. Khasanov, R.; Castro, D.D.; Belogolovskii, M.; Paderno, Y.; Keller, H. Anomalous electron-phonon coupling probed on the surface of superconductor ZrB_{12}. *Phys. Rev. B* **2005**, *72*, 224509. [CrossRef]
18. Daghero, D.; Gonnelli, R.S.; Ummarino, G.A.; Calzolari, A.; Dellarocca, V.; Stepanov, V.A.; Filippov, V.B.; Paderno, Y.B. Andreev-reflection spectroscopy in ZrB_{12} single crystals. *Supercond. Sci. Technol.* **2004**, *17*, S250. [CrossRef]
19. Gasparov, V.A.; Sidorov, N.S.; Zver′kova, I.I. Two-gap superconductivity in ZrB_{12}: Temperature dependence of critical magnetic fields in single crystals. *Phys. Rev. B* **2006**, *73*, 94510. [CrossRef]
20. Nicol, E.J.; Carbotte, J.P. Properties of the superconducting state in a two-band model. *Phys. Rev. B* **2005**, *71*, 054501. [CrossRef]
21. Gasparov, V.; Sheikin, I.; Levy, F.; Teyssier, J.; Santi, G. The de Haas van Alphen effect study of the Fermi surface of ZrB_{12}. *J. Phys. Conf. Ser.* **2009**, *150*, 052059. [CrossRef]
22. Wang, Y.; Lortz, R.; Paderno, Y.; Filippov, V.; Abe, S. Specific heat and magnetization of a ZrB_{12} single crystal: Characterization of a type-II/1 superconductor. *Phys. Rev. B* **2005**, *72*, 24548. [CrossRef]
23. Ge, J.Y.; Gutierrez, J.; Lyashchenko, A.; Filipov, V.; Li, J.; Moshchalkov, V.V. Direct visualization of vortex pattern transition in ZrB_{12} with Ginzburg-Landau parameter close to the dual point. *Phys. Rev. B* **2014**, *90*, 184511. [CrossRef]
24. Huebener, R.P. The path to type-II superconductivity. *Metals* **2019**, *9*, 682. [CrossRef]
25. Zhang, A.L.; Gao, L.X.; He, J.Y.; Filipov, V.B.; Cao, S.; Xiao, Q.L.; Ge, J.Y. Experimental evidence for type-1.5 superconductivity in ZrB_{12} single crystal. *Sci. China Phys. Mech. Astron.* **2022**, *65*, 297412. [CrossRef]
26. Tang, L.; Zhang, J.; Jin, Y.; Kong, P.; Li, S.; Huo, D.; Zhang, C.; Kuang, F. Pressure-induced novel phases with the high-T_c superconductivity in zirconium dihydride. *Mater. Today Commun.* **2024**, *40*, 109516. [CrossRef]
27. Li, Y.; Gao, Y.; Han, Y.; Liu, C.; Peng, G.; Wang, Q.; Feng, K.; Ma, Y.; Gao, C. Metallization and hall-effect of Mg_2Ge under high pressure. *Appl. Phys. Lett.* **2015**, *107*, 142103. [CrossRef]
28. Thakur, S.; Biswas, D.; Sahadev, N.; Biswas, P.K.; Balakrishnan, G.; Maiti, K. Complex spectral evolution in a BCS superconductor, ZrB_{12}. *Sci. Rep.* **2013**, *3*, 3342. [CrossRef]
29. Thakur, S.; Maiti, K. Unusual correlation physics in a BCS superconductor, ZrB_{12}. *Solid State Commun.* **2014**, *193*, 45–50. [CrossRef]
30. Escamilla, R.; Romero, M.; Morales, F. Elastic properties, Debye temperature, density of states and electron–phonon coupling of ZrB_{12} under pressure. *Solid State Commun.* **2012**, *152*, 249–252. [CrossRef]
31. Yamaura, K.; Huang, Q.; Akaishi, M.; Takayama-Muromachi, E. Superconductivity in the hexagonal-layered molybdenum carbide η-Mo_3C_2. *Phys. Rev. B* **2006**, *74*, 184510. [CrossRef]
32. Silaev, M.; Babaev, E. Microscopic theory of type-1.5 superconductivity in multiband systems. *Phys. Rev. B* **2011**, *84*, 094515. [CrossRef]
33. Bolotina, N.B.; Khrykina, O.N.; Azarevich, A.N.; Shitsevalova, N.; Filipov, V.B.; Gavrilkin, S.Y.; Mitsen, K.V.; Voronov, V.V.; Sluchanko, N.E. Checkerboard patterns of charge stripes in the two-gap superconductor ZrB_{12}. *Phys. Rev. B* **2022**, *105*, 054511. [CrossRef]
34. Biswas, P.K.; Rybakov, F.N.; Singh, R.P.; Mukherjee, S.; Paul, D.M.K. Coexistence of type-I and type-II superconductivity signatures in ZrB_{12} probed by muon spin rotation measurements. *Phys. Rev. B* **2020**, *102*, 144523. [CrossRef]
35. Li, X.; Yong, Y.; Cui, H.; Zhang, R. Mechanical behavior, electronic and phonon properties of ZrB_{12} under pressure. *J. Phys. Chem. Solids* **2018**, *117*, 173–179. [CrossRef]